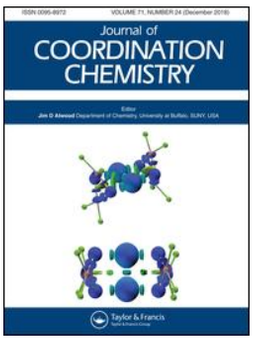

Journal of Coordination Chemistry

ISSN: 0095-8972 (Print) 1029-0389 (Online) Journal homepage: https://www.tandfonline.com/loi/gcoo20

Synthesis, characterizations, crystal structures, BSA-binding, molecular docking and cytotoxic activities of nickel(II) and copper(II) coordination complexes with bidentate N,S-chelating ligand

Noorussabah, Mukesh Choudhary, Achintya Jana, Neeladri Das, B. Mohan, K. Ahmad, Sangeeta, S. Bharti, M. K. Mishra & S. R. Sharma

To cite this article: Noorussabah, Mukesh Choudhary, Achintya Jana, Neeladri Das, B. Mohan, K. Ahmad, Sangeeta, S. Bharti, M. K. Mishra & S. R. Sharma (2019): Synthesis, characterizations, crystal structures, BSA-binding, molecular docking and cytotoxic activities of nickel(II) and copper(II) coordination complexes with bidentate N,S-chelating ligand, Journal of Coordination Chemistry, DOI: 10.1080/00958972.2019.1602867

To link to this article: https://doi.org/10.1080/00958972.2019.1602867

Accepted author version posted online: 01 Apr 2019.

Synthesis, characterizations, crystal structures, BSA-binding, molecular docking and cytotoxic activities of nickel(II) and copper(II) coordination complexes with bidentate N,S-chelating ligand

NOORUSSABAH†, MUKESH CHOUDHARY1†, ACHINTYA JANA‡, NEELADRI DAS‡, B. MOHAN†, K. AHMAD†, SANGEETA†, S. BHARTI†, M. K. MISHRA† and S. R. SHARMA†

†Department of Chemistry, National Institute of Technology Patna, Patna 800005, India
‡Department of chemistry, Indian Institute of Technology Patna, Patna 801106, India

In the present investigation, we report the synthesis and characterization of three novel nickel(II) [Ni(L)$_2$] (**1**) and copper(II) [Cu(L)$_2$] (**2a**) and [Cu(L)$_2$] (**2b**) complexes, which are made through the coordination of (*E*)-1-(2-methoxybenzylidine)-4-phenylethiosemicarbazone (HL) as bidentate N,S-ligand. Several modern techniques including experimental electronic and fluorescence spectroscopy, single-crystal X-ray crystallography, molecular docking and BSA-binding are used to characterize the isolated coordination compounds. X-ray crystallography, FT-IR and UV-visible spectra agree with the observed crystal structures. The crystallographic and spectroscopic studies confirmed that these complexes display four-coordinate square planar *trans*-[MN$_2$S$_2$] coordination geometry, whose central metal(II) atom lies on the center of symmetry. Complexes **1** and **2a** crystallized in the orthorhombic system of the space group *Pbca* whereas **2b** crystallized in the monoclinic system of P2$_1$/c. The binding affinity of complexes towards bovine serum albumin (BSA) was determined by UV-visible and fluorescence spectrophotometric methods. The cytotoxic/antiproliferative potential of the synthesized compounds on human cell lines was also investigated by MTT assay.

1Corresponding author. Email: mukesh@nitp.ac.in

Graphical abstract

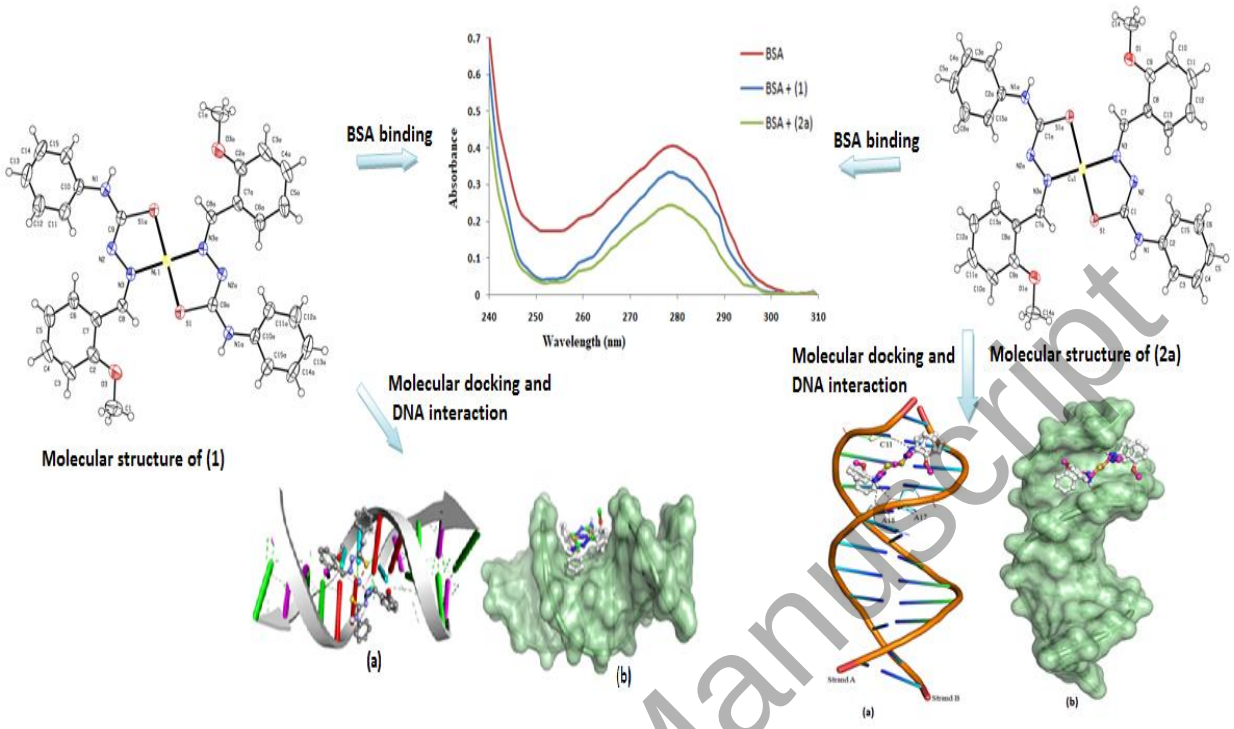

Keywords: Coordination complexes; BSA Binding studies; Molecular docking; Protein interaction; Cytotoxic studies

1. Introduction

The synthesis and study of low molecular weight coordination complexes of nickel(II) and copper(II) bound by nitrogen and sulfur ligands are very important because of their pivotal roles in bioinorganic chemistry, potential catalytic applications [1-4] and BSA binding [5, 6]. Over the last few decades, thiosemicarbazones and their metal complexes have received considerable attention in view of their structural diversity, variable binding modes, and promising biological implications [7-9]. Thiosemicarbazone and/or 4-phenylthiosemicarbazide derived Schiff bases possess a wide range of biological properties and they act as antibacterial, antifungal, antitumor, anticancer and anti-inflammatory agents [10-12]. The biological activity of thiosemicarbazone is related to its chelating ability with transition metal ions, and its coordination to metal ions through nitrogen and sulfur atoms allows it to act as a potent cytotoxic compound and enhance

the biological activity [13, 14]. The deprotonated thiosemicarbazone ligands usually coordinate to Pt(II), Pd(II), Cu(II), Ru(II) and Os(II) through N,S-donor atoms in their bidentate form or tridentate form, to form metallic complexes of different molecular geometry [15, 16]. The square planar Pt(II) and Pd(II) complexes with thiosemicarbazone ligands derived from phenylacetaldehyde and 2-formylpyridine showed high cytotoxicity *in vitro* against HL60 leukemia and P388 mouse leukemia cell lines [17], while Pt(II) and Pd(II) complexes with *p*-isopropylbenzaldehyde thiosemicarbazone ligands exhibit strong cytotoxic activities on mouse tumor cell growth inhibition [18]. Jayabalakrishnan *et al.* [19] reported two 4-phenyl-3-thiosemicarbazone ligands and its Ru(II) complexes focused on the binding and cleavage properties with CT-DNA. The interesting observation was that in all the complexes reported by them the *in vitro* cytotoxicity of the ligands and complexes assayed against HeLa and MCF-7 cell lines showed higher cytotoxic activity with the lower IC_{50} values indicating their efficiency in killing the cancer cells even at low concentrations. Casas *et al.* [20] reported a series of dimethyl Tl(III) complexes of acetylferrocene thiosemicarbazonates as a N,S-chelating ligand, forming either a four-membered or a five-membered chelate ring depending on the substituent on the N(4) atom. The four-membered chelate rings were also observed [21-23] for organometallic derivatives of group 13 elements (Al, Ga and In), for Pd as well as other dimethyl Tl(III) and Ru(II) complexes [24].

DNA is the primary target molecule for most anticancer drugs as it regulates many biochemical processes occurring in the cellular system. Many small molecules exert their anticancer effect by interfering with DNA-replication leading to cell death through apoptosis. Binding studies of small molecules to DNA are very important in the development of new therapeutic reagents and DNA molecular probes [25]. It has been shown that the α-(*N*)-heterocyclic carbaldehyde thiosemicarbazones act as chelating agents of the transition metals and some of them exhibit antitumor activity by inhibiting the biosynthesis of DNA, possibly by blocking the enzyme ribonucleotide diphosphate reductase [26, 27]. In particular, ruthenium(II) organometallics represent one of the latest trends in metallodrug research [28]. Among these DNA-targeted guest molecules, copper(II)- and nickel(II)-based compounds have attracted much attention because of low toxicity and their promising anticancer activity [29-31], DNA-binding and -cleavage activity [32], metallodrugs [33]. Bovine serum albumin (BSA) has been widely used as a model protein to study drug protein interactions due to its structural similarity with

human serum albumin (HSA), its low cost, stability, ease of purification, abundance and ligand binding properties [34]. Schiff base metal complexes can bind to BSA with high affinity, thereby quenching BSA's intrinsic fluorescence and inducing conformational changes [35].

Literature reveals that the syntheses and structural studies of Cu(II) and Ni(II) complexes of 2-methoxybenzylidine derivative of 4-phenylthiosemicarbazide with molecular docking into the grooves of target DNA- and BSA-binding is missing and, to date, no further investigations are considered; this impelled us to make the present study. Inspired by recent studies on metal-coordinated Schiff bases for their BSA- and protein-binding [35, 37] and based on our good experience on Schiff base Ni(II) and Cu(II) coordinated complexes [38-41], in this paper we plan to synthesize, characterize as well as to study their molecular docking and BSA-binding of three novel nickel(II) $[Ni(L)_2]$ (**1**) and copper(II) $[Cu(L)_2]$ (**2a**) and $[Cu(L)_2]$ (**2b**) complexes with (E)-1-(2-methoxybenzylidine)-4-phenylethiosemicarbazone (HL) as bidentate N,S-ligand. A solid-state structure is planned to be determined by X-ray analysis. The crystal structure determination also confirmed that the structures of all complexes are isostructural. The refined single-crystal structures are further subjected to molecular docking into the grooves of target DNA and binding affinity of complexes with the DNA and interacting residues of DNA was evaluated and discussed. Further protein binding constant (K_b), quenching constant (K_{SV}) and number of binding sites (n) of complexes towards BSA was determined by using fluorescence spectroscopy. The cytotoxic/antiproliferative potential of the synthesized compounds on human cell lines was also investigated by MTT assay.

2. Experimental

2.1. *Materials*

Chemicals used were of analAR grade. 4-Phenyl-thiosemicarbazide, 2-methoxy-benzaldehyde, $Ni(OAc)_2 \cdot 4H_2O$, $Cu(OAc)_2 \cdot H_2O$ and $Cu(NO_3)_2 \cdot 3H_2O$ were obtained from Sigma. Human embryonic kidney (HEK293), human heptoma cells (HepG2) and human prostate carcinoma (LNCaP) cells were procured from National Centre for Cell Sciences, Pune, India. Dulbecco's modified eagle's media (DMEM), RPMI-1640 medium, antibiotic cocktail and fetal bovine serum (FBS), TrypLE™ Express enzyme solution and MTT (3-[4,5-dimethylthiazol-2-yl]-2,5-diphenyltetrazolium bromide) were obtained from Gibco-life Technologies, Thermo Fisher Scientific (USA). Used solvents were dried and purified as reported standard methods [42, 43].

2.2. ***Preparations***

2.2.1. Synthesis of (E)-1-(2-methoxybenzylidine)-4-phenylethiosemicarbazone (HL). The ligand HL was synthesized according to an analogous method reported earlier [44, 45]. HL, a bidentate N,S-ligand, was synthesized by refluxing equimolar mixtures of 4-phenylthiosemicarbazide (10 mmol, 1.67 g) and 2-methoxybenzaldehyde (10 mmol, 1.36 g) in dry methanol at 55-60 °C for 3 h. A colorless solution was obtained and was left overnight. The colorless crystalline product of HL was obtained, filtered off, washed with ethanol, and stored in a desiccator over $CaCl_2$. The Schiff base HL gave satisfactory elemental analysis. Yield: 2.48 g (82%). Color: colorless, melting point: 178 °C. Anal. Calc. for $C_{15}H_{15}N_3OS$, HL (%): C, 63.11; H, 5.29; N, 14.70. Found (%): C, 63.13; H, 5.30; N, 14.73. FAB-mass (m/z): Obs. (Calcd): 285.09 (286).

2.2.2. Synthesis of $[Ni(L)_2]$ (1). HL (2.0 mmol, 0.570 g) was dissolved in ethanol (20 mL) in the presence of triethylamine (3.0 mmol, 40 µL) and was combined with $Ni(OAc)_2 \cdot 4H_2O$ (1.0 mmol, 0.249 g) with constant stirring and heating (60 °C). On cooling the solution to room temperature, green crystals suitable for single-crystal X-ray diffraction were recovered from mother liquor which were filtered off, washed with ethanol and stored in a desiccator over $CaCl_2$. Yield: 0.57g (70%). Color: green, melting point: 240 °C. Anal. Calc. for $C_{30}H_{28}NiN_6O_2S_2$ (**1**) (%): C, 57.40; H, 4.47; N, 13.37. Found: C, 57.43; H, 4.50; N, 13.39. FAB-mass (m/z): Obs. (Calcd): 627.41 (628).

2.2.3. Synthesis of $[Cu(L)_2]$ (2a). HL (2.0 mmol, 0.570 g) was dissolved in ethanol (20 mL) in the presence of triethylamine (3.0 mmol, 40 µL) and was combined with $Cu(OAc)_2 \cdot H_2O$ (1.0 mmol, 0.1998 g) with constant stirring and heating (70 °C). On cooling the solution to room temperature, light-brown crystals separated and were filtered off, washed with MeOH and stored in a $CaCl_2$ desiccator. Complex **2a** gave satisfactory elemental analysis. Yield: 0.524 g (76%). Color: light blue, melting point: 208 °C, Anal. Calc. for $C_{30}H_{28}CuN_6O_2S_2$ (**2a**) (%): C, 56.95; H, 4.45; N, 13.27. Found: C, 56.99; H, 4.46; N, 13.29. FAB-mass (m/z): Obs. (Calcd): 632.25(633).

2.2.4. Synthesis of [Cu(L)$_2$] (2b). To an ethanol solution (20 mL) of $Cu(NO_3)_2 \cdot 3H_2O$ (1.0 mmol, 0.241 g) was stirred with ethanol solution of HL (2.0 mmol, 0.570 g) continuously for 3 h after adding 2 drops of triethylamine. To the above reaction mixture, ammonium thiocyanate (2.0 mmol, 0.116 g) in MeOH (20 mL) was added with constant stirring. One minute later, pink color turned to pink-red and the odor of ammonium thiocyanate was detected. The pink-red crystals suitable for single-crystal X-ray diffraction were recovered from mother liquor and were filtered off, washed with MeOH, and stored in a desiccator over $CaCl_2$. Complex **2b** gave same elemental analysis as **2a**. The basic difference between the structures of **2a** and **2b** was that **2a** was crystallized in the orthorhombic system of space group *Pbca* whereas **2b** crystallized in the monoclinic system of the space group *P21/c*.

2.3. *Physical measurements*

Elemental analyses were made on an ElementarVario EL III Carlo Erba 1108 analyzer. FAB mass spectra were recorded on a JEOL SX 102/DA 6000 mass spectrometer using xenon (6 kV, 10 mA) as the FAB gas. The accelerating voltage was 10 kV and the spectra were recorded at room temperature (RT) with m-nitro-benzoyl alcohol as the matrix. Magnetic susceptibility measurements of powder samples of complexes were made on a Gouy balance using a mercury(II) tetrathiocynato cobaltate(II) as calibrating agent ($\chi_g = 16.44\times10^{-6}$ c.g.s. units). All the experimental data were corrected for diamagnetic contributions, which were estimated from Pascal's tables, and temperature-independent paramagnetism (TIP). The molar ion exchange was measured using a systronics digital conductivity meter (TDS-308) using a 10^{-3} M solution in DMSO. FT-IR spectra were recorded on a Shimadzu IRAffinity-1S Fourier Transform Infrared Spectrophotometer from 4000-400 cm^{-1} on KBR pellets. UV-visible spectra were obtained on a Thermo scientific Evolution-300 spectrophotometer. Fluorescence spectroscopic data were measured on a Fluoromax-4 Spectro-fluorometer. Single-crystal X-ray structure determination was carried out on a Bruker Smart 1000 CCD area detector diffractometer.

2.4. *X-ray crystallographic analysis*

Crystals suitable for single-crystal X-ray analysis for **1**, **2a** and **2b** were grown by slow evaporation of the reaction mixture at room temperature. Single-crystals suitable for single-crystal X-ray analysis were mounted on glass fibers and data were collected on a Bruker Smart

CCD detector using graphite monochromated Mo Kα radiation (λ = 0.71073 Å) at 296 K. The structures were solved by direct methods using SHELXS-97 [46] and refined by full-matrix least-square techniques [47] against F^2 using SHELXL-97. All non-hydrogen atoms were refined using anisotropic thermal parameters. Hydrogens were geometrically fixed and allowed to refine isotropically. Crystallographic data for the structures reported in this paper have been deposited with the Cambridge Crystallographic Data Centre (CCDC) as supplementary publication numbers CCDC 1565755, 1836258 and 1837668 for **1**, **2a** and **2b**, respectively.

2.5. *Protein-binding studies*

The protein binding of **1** and **2a** with BSA was studied by fluorescence spectra recorded at a fixed excitation wavelength corresponding to BSA at 280 nm and monitoring the emission at 348 nm. The excitation and emission slot widths and scan rates were maintained constant for all the experiments [48]. Stock solution of BSA was prepared in 50 μM phosphate buffer (pH = 7.2) and stored in the dark at 4 °C for further use. Concentrated stock solutions of each test compound were prepared by dissolving them in DMF-Phosphate buffer (5:95) and diluted with phosphate buffer to get required concentrations. 2.5 mL of BSA solution was titrated by successive addition of a 10^{-6} M stock solution of the complexes using a micropipette. In UV-visible absorption experiment, a fixed concentration of BSA was titrated with increasing concentration of complexes.

2.6. *Molecular docking studies*

Molecular docking investigations of **1** and **2a** have highlighted the accurate and preferred orientation of the compounds at the binding sites of the DNA. These dimensional coordinates of target DNA (duplex of sequence d(CGCGAATTCGCG)2 dodecamer) were taken from protein Data Bank with PDB ID IBNA. The given compounds were used for docking studies with DNA to predict the bound confirmations the binding affinities. AutoDock4 [49] and Auto Dock Vina [50] were used for docking purpose. PyMol [51], Discovery Studio Visualizer [52] and LigPlot$^+$ [53] were used for visualization purpose to visualize the different interactions between the target and given compounds.

2.7. *Cell culture and cytotoxicity studies*

HEK293 and HepG2 cells were maintained and cultured in DMEM media and LNCaP cells were cultured in RPMI-1640 medium (supplemented with 10% heat inactivated FBS and 1% penicillin, streptomycin solution) in a humidified incubator (5% CO_2) at 37 °C. The cultures of each cell line were maintained and trypsinized not more than 30 passages, after the revival of cryostocks. The cytotoxicity of each compound was evaluated with the help of MTT assay as described earlier [54, 55]. Briefly, the cells were plated (9000-10000 cells/well) in a 96-well cell culture plate and grown overnight. Next day, to each cell line the treatment were given with increasing concentrations (0–200 μg/mL) of the compounds for 72 h at 37 °C in a CO_2 incubator. After 72 h, the mixture of cell culture medium and compounds were pipetted out and cells were washed three times using phosphate buffer saline (pH 7.4). Subsequently, 20 μL of MTT solution (from 5 mg/mL stock solution in PBS) and 100 μL of cell culture medium were added to each well and incubated for 4-5 h at 37 °C in the CO_2 incubator. After 4-5 h incubation, the supernatant was removed and the purple formazan crystals were dissolved by adding 150 μL DMSO to each well. The absorbance was measured at 570 nm on a multi-plate ELSIA reader (BioRad). The percentage of cell viability was calculated and plotted as a function of concentration of compound. For anticancer studies paclitaxel was taken as positive control.

3. Results and discussion

3.1. *Synthesis and characterization*

The main idea of the present work is to synthesize, characterize as well as to study their biological investigations of three novel nickel(II) $[Ni(L)_2]$ (**1**) and copper(II) $[Cu(L)_2]$ (**2a**), $[Cu(L)_2]$ (**2b**) complexes, which are formed through the combination of (E)-1-(2-methoxybenzylidine)-4-phenylethiosemicarbazone (HL) as bidentate N,S-ligand. In the first step, Schiff base HL was prepared by the reaction between 4-phenylthiosemicarbazide and 2-methoxybenzaldehyde in a ratio of 1:1 (scheme 1). Finally, the Schiff base (HL) reacted with $Ni(OAc)_2{\cdot}4H_2O$, $Cu(OAc)_2{\cdot}H_2O$, $Cu(NO_3)_2{\cdot}3H_2O$ in a ratio of 2:1 to afford **1**, **2a** and **2b**, respectively. The protocol used for the synthesis of HL and its complexes is given in scheme 1. Suitable crystals were selected for single-crystal X-ray analysis. The synthesis and characterization of HL and its complexes are still rare, which indicates the novelty of the present work. The obtained complexes were microcrystalline solids and they were stable in air with

melting points above 200 °C. They were insoluble in water and methanol but soluble in organic solvents such as acetonitrile, chloroform, DMF and DMSO. These complexes displayed a four-coordinate tetrahedral or square planar trans-[MN_2S_2] coordination geometry whose central metal(II) atoms lie on the center of symmetry. The elemental analysis and crystal structures were in agreement with the chemical formula proposed for all complexes. The observed molar conductance value of the complexes in acetonitrile (1×10^{-3} M) suggest a non-electrolyte nature [56] due to the low conductivity values [Λ_M = 18 $\Omega^{-1}cm^2$ mol^{-1}: 150 for **2a** and **2b**] except **1** which was electrolyte in nature. Complex **1** behaves as 1:2 electrolyte in MeCN solution (Λ_M = 220 $\Omega^{-1}cm^2$ mol^{-1}), indicating the thiosemicarbazone ligand act as neutral N,S-donors in this complex. Room temperature magnetic moment measurements of the complexes at 298 K indicate they are paramagnetic. As **1** was found to be paramagnetic, what excludes a square planar configuration? The general rule that in Ni(II) d^8 chemistry, tetrahedral (or nearly tetrahedral) complexes have temperature-dependent magnetic moments which are usually higher than the spin-only value while the square-planar complexes are diamagnetic, therefore the value of magnetic moment would be zero. At 298 K, the calculated value of magnetic moment (μ_{eff}) was 2.35 BM for **1** and 1.68 BM for **2a** and **2b**. These magnetic moment values lie within the range normally found for other four-coordinate tetrahedral nickel(II) complexes [57] and/or square-planar copper(II) complexes [58].

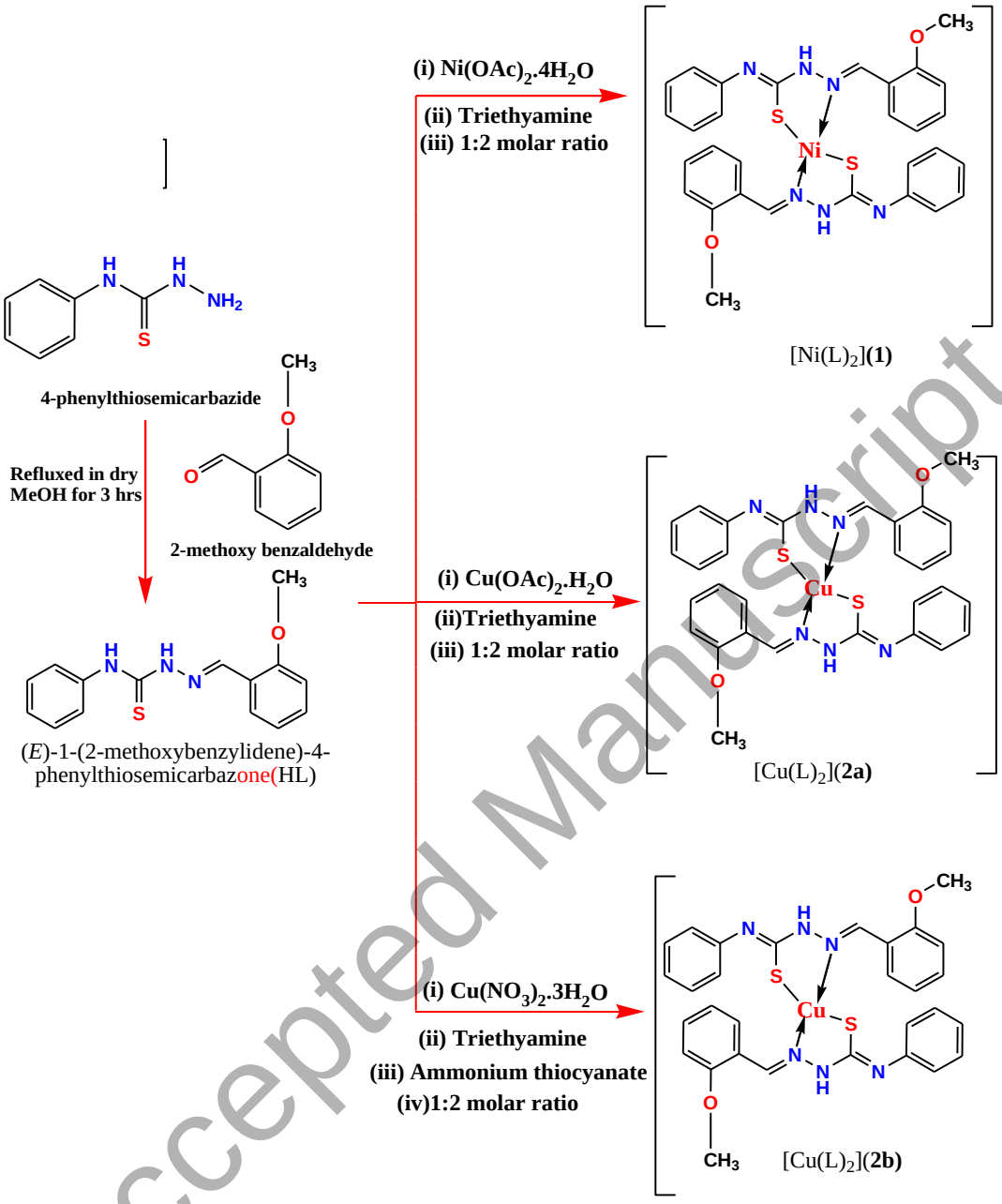

Scheme 1. Synthetic route for HL and its mononuclear Ni(II) and Cu(II) complexes.

3.2. *Crystal structure description*

The molecular structure of **1**, **2a** and **2b** along with the atomic numbering scheme is given in figures 1-3, respectively. Crystal data and some selected bond lengths and angles are summarized in tables 1 and 2, respectively. Single-crystal X-ray diffraction reveals that the complexes are mononuclear. The crystal structure determinations also confirm that the structures

of **1**, **2a** and **2b** are isostructural. The single-crystal X-ray diffraction study reveals that **1** crystallized in the orthorhombic crystal system with space group *Pbca* [a = 15.4786(11) Å, b = 7.6422(5) Å, c = 24.613(2) Å, α = 90°, β = 90°, γ = 90°, Z = 4]. Here the E-configuration of HL in the solid state is illustrated for its coordination with the metals as monobasic bidentate with N- and S-donor groups suitably oriented for forming five-membered chelate ring. The symmetry around nickel(II) in **1** can be described as square planar, the nickel(II) ion is bonded to monobasic bidentate N,S-donor ligand forming a type of tetradentate N_2S_2-donor bis-Schiff base complex, thus constructing two five-membered chelate rings [1.Ni(1)-N(3)-N(2)-C(9)-S(1a), 2.Ni(1)-N(3a)-N(2a)-C(9a)-S(1)]. The Ni-N(imine) bond distances are 1.91 Å and 2.17 Å in **1**, which is very close to the reported Ni-N(imine) bond distances for Ni(II) complexes having perfect square planar geometry [59-61]. The Ni(II) of **1** has crystallographic inversion symmetry (symmetry code: -x, -y, -z) to offer a square planar geometry and axial positions are vacant. As shown in figure 1, the perfect geometry may conveniently be measured by the *trans* angles that are ideally 180° for **1**; N(3)-Ni-N(3a) = 180° and S(1)-Ni-S(1a) = 180°. Similar observations have been made by Kundu *et al.* [62].

Complexes **2a** and **2b** afford a four-coordinate square planar *trans*-[MN_2S_2] coordination geometry whose central metal atom lies on the center of symmetry. The X-ray structural studies of **2a** and **2b** reveal that the metal complex has 2:1 ligand-to-metal stoichiometry, crystallized in orthorhombic and monoclinic system in the space group Pbca and P21/c, respectively [a = 15.507(3) Å, b = 7.5988(16) Å, c = 24.876(5) Å, α = 90°, β = 90°, γ = 90°, Z = 4 for **2a** and a = 19.141(7) Å, b = 7.667(3) Å, c = 22.470(9) Å, α = 90°, β = 104.803, γ = 90°, Z = 4 for **2b**] and consist of a Cu(II) and two monobasic bidentate chelating ligand L. Both the N and the S atoms of L are at special positions on the perpendicular axes, and the point of intersection of coordinated axes is the Cu(II) ions. The basal plane of the square plane is bound by two N atoms from C=N groups, N(3), N(3a) for **2a**, N(3), N(6) for **2b** and two S atoms from thiol group S(1), S(1a) for **2a** and S(1), S(2) for **2b**, forming a type of tetradentate N_2S_2-donor, bis-Schiff base complex, thus constructing two five-membered chelate rings [1. Cu(1)-S(1a)-C(1a)-N(2a)-N(3a), 2.Cu(1)-S(1)-C(1)-N(2)-N(3)] for **2a** and [1.Cu(1)-S(1)-C(2a)-N(2)-N(3), 2.Cu(1)-S(2)-C(1)-N(4)-N(5) for **2b**. As shown in figures 2 and 3, **2a** and **2b** have similar solid structure, and the metal centers were coordinated to two imine-N and bounded to two thiol-S atoms being deprotonated in *trans*-confirmation whereas the metals are situated on inversion centers to form a

distorted square planar [63]. As they are crystallographically centrosymmetric, the perfect symmetry may conveniently be measured by *trans* angles [S(1)-Cu(1)-S(1) = 180°, N(3)-Cu(1)-N(3) = 180° for **2a** and N(3)-Cu(1)-N(6) = 159.6°, S(1)-Cu(1)-S(2) = 156.32° for **2b**] that are ideally 180° for square planar complexes [64]. The Cu-N bond distances were 2.008 Å in **2a** and 1.993(4) Å in **2b** which are located in the range of known values for Cu-N(imine) bonds in analogous square planar Cu(II) species [65]. While formation of **2a** required use of $Cu(OAc)_2 \cdot H_2O$ and triethylamine, the formation of **2b** required use of $Cu(NO_3)_2 \cdot 3H_2O$, triethylamine and ammonium thiocynate. The yield of **2a** and **2b** was the same with molecular formula and the only difference is their crystallographic space groups [orthorhombic with *Pbca* for **2a** and monoclinic with $P2_1/c$ for **2b**], therefore **2a** and **2b** are highly isostructural. Further, it is assumed that counter anion and SCN^- ions have no significant role in the complexation of **2b**. As shown in figures S1-S3, in crystal structures of complexes, there are no remarkable intermolecular hydrogen bonds and intermolecular π---π interaction within van der Waals radii. Thus, the crystal packing may be dominated by non-covalent and weak van der Waals forces. The molecular arrangement and anti-parallel orientation of the molecular planes shows one-dimensional chains along the crystallographic *c*-axis. The unit cell packing diagrams of the complexes are graphically presented in figures S1-S3, along with *c*-axis.

3.3. *FT-IR and UV-visible spectroscopy*

The FT-IR spectra of Schiff base (HL) and its complexes $[Ni(L)_2]$ (**1**), $[Cu(L)_2]$ (**2a**) and $[Cu(L)_2]$ (**2b**) were recorded from 400 to 4000 cm^{-1} at room temperature. Characteristic IR bands for HL are different from those of the complexes providing significant information regarding the bonding sites of the thiosemicarbazone ligand to the metals. Some representative IR spectra of HL and its complexes are given in the Supplementary Material (figures S4-S6). In the IR spectrum of HL the highest frequency bands at 3277 cm^{-1}, 3142 cm^{-1} and 2999 cm^{-1} may be assigned to the asymmetric *ν*(N-H) vibrations and symmetric *ν*(N-H) vibrations of the imino- and amino-groups, respectively [66]. These *ν*(N-H) vibrations shifted to higher frequencies (3379-3380 cm^{-1}) in all the complexes at the same positions compared to that of HL indicates that free *ν*(N-H) vibrations do not participate in coordination. A band appeared at 1249 cm^{-1} for HL due to vibration of the C=S double bond which disappeared in the spectra of the complexes and a new band appeared at 1244 cm^{-1} for **1**, 1242 cm^{-1} for 2**a** and **2b**, indicating that the other coordination

is through thiolate sulphur after enolization followed by deprotonating on sulphur [67, 68]. Free HL shows a sharp intense band at 1593 cm^{-1} assigned to the *ν*(C=N) of azomethine group. This band shifted to higher frequencies at 1597 cm^{-1} in all the complexes, indicating coordination of azomethine nitrogen of ligand to the metal ion [69]. The IR data of HL and its complexes **1**, **2a** and **2b** showed that HL was coordinated to the metal ion in a monobasic bidentate-N,S manner (L). The infrared spectra of HL and their complexes agree with the observed crystal structures shown in figures 1-3.

The nature of ligand and field around the metal ion was deducted from the electronic spectra. UV-visible absorption spectra of HL and its complexes **1**, **2a** and **2b** were recorded from 200-800 nm using DMSO as solvent at 25 °C. Representative UV-vis spectra of HL and its complexes are depicted in figure 4. The UV-visible spectra of thiosemicarbazone (HL) showed two absorption bands 325 and 342 nm due to π-π* and n-π* transitions, respectively. The electronic spectrum of **1** displayed two bands of 359 nm and 576 nm, which are assigned to $^1A_g \rightarrow {}^1E_g$ (n_1) and $^1A_{1g} \rightarrow {}^1B_{2g}$ (n_2) transitions, respectively. This complex is paramagnetic in nature; therefore, four-coordinate tetrahedral geometry [70] is suggested. The electronic spectrum of **2a** of HL shows two bands at 270 and 574 nm, which was assigned to the $^2B_{1g} \rightarrow {}^2B_{2g}$ and $^2B_{1g} \rightarrow {}^2Eg$ transitions, respectively. Since the value of magnetic moment was 1.68 BM, a four-coordinate square planar geometry [71] was suggested for **2a**. Similar electronic spectrum was observed for **2b** of HL.

3.4. *Protein binding and molecular docking studies*

The absorption spectra of protein (BSA) were obtained in presence of metal complexes **1** and **2a** to predict the type of quenching process. Some representative fluorescence curve of BSA in the presence and absence of complexes is graphically presented in figures 5, S7 and S8. Quenching mainly occurs through either static or dynamic modes. Dynamic quenching refers to the process in which quencher and fluorophore come in contact during excited state, whereas in static quenching they come in contact during ground state. The obtained electronic spectra showed that the absorption intensity of BSA was enhanced upon addition of **1** and **2a**. This result suggested that the binding of metal complexes with BSA was through a static quenching mode [72]. The interaction of **1** and **2a** and BSA were also observed through fluorescence spectral method. A solution of BSA (1 μM) was titrated with various concentrations of metal complexes (0 μM –

25 mM) and the spectra were obtained in the range of 300-400 nm upon excitation at 280 nm. With the increase in concentrations of metal complexes, the characteristic fluorescence emission band of BSA at 335 nm was quenched in a consistent manner, along with a bathochromic shift of around 2-5 nm. The observed bathochromic shift is due to the fact that the active site in BSA is suppressed in a hydrophobic environment [73]. The above results suggested that a strong interaction occurred between the metal complexes and BSA. To assess the interaction between the metal complexes and BSA, Stern-Volmer (figure S9) and Scatchard plots (figure S10) were used. The Stern-Volmer quenching relation is given by following equation:

$$I_0/I = K_{SV}[Q] + 1 \quad (1)$$

where I_0 is the emission intensity in the absence of the quencher, I is the emission intensity in the presence of the quencher, [Q] is the concentration of quencher and K_{SV} is the Stern-Volmer quenching constant. The quenching constant (K_{SV}) can be calculated using the plot of I_0/I *versus* [Q] (figure S9). When a small drug molecule binds to a set of equivalent sites on a macromolecule, the equilibrium between free and bound molecules is represented by the Scatchard equation [74]:

$$\log [(I_0-I)/I] = \log K_b + n \log[Q] \quad (2)$$

where K_b is the binding constant of the complex with BSA and n is the number of binding sites. From the plot of log $[(I_0-I)/I]$ *versus* log[Q] (figure S10), the binding constant (K_b) and the number of binding sites (n) have been obtained. The binding constant (K_b), quenching constant (K_{SV}), and the number of binding sites (n) for the interaction of **1** and **2a** with BSA are given in table 3. The observed results clearly indicate that **1** and **2a** have only one binding site to interact with BSA and the binding constant values for **1** is more than that of **2a**.

Molecular docking study gives the accurate and preferred orientations of the chemical compound at the binding site of the receptor. Here, in molecular docking studies, we found that **1** and **2a** were docked into the grooves of target DNA and resulted docked conformations were selected on the basis of obtained interaction energy parameters and scoring functions (table 4). Conformations of docked compounds with DNA are shown in figures 6 and 7, showing the interactions between complexes and target DNA. Complex **1** shows a little higher free energy of

binding with DNA (-8.3 kcal/mol) as compared to **2a**, which shows -8 kcal/mol binding free energy. Both **1** and **2a** bind to the DNA showing little difference in their binding affinities due to the differences between the metals by which these complexes are linked [75]. Complex **1** was found to interact with C3, G4, A5, A6 and T7 of strand A, G16, A17, A18, T19 and T20 of strand B of DNA and forming a hydrogen bond with A5 of strand A. Complex **2a** shows several close interactions with C9, G10, C11 and G12 of strand A, and G14, C15, G16, A17 and A18 of strand B of target DNA, where three hydrogen bonds are forming with C11 of strand A and A17, A18 of strand B of the DNA.

3.5. *Cytotoxicity studies*

To study the cytotoxic/antiproliferative potential of synthesized compounds on human cell lines, MTT assay was used as it is a widely used method to evaluate the number of viable cells in a particular format of treatment. This assay is based on the observation that viable cells having active metabolism can convert MTT into purple formazan having absorbance maxima at 570 nm, however, dead cells do not have the capability to convert MTT into formazan [76]. The compounds were screened in the concentration range of 0-200 µg/mL, and treatments were given for 72 h. Interestingly, the treatment of these compounds does not affect the viability of HEK293 cells, but in the case of LNCaP and HepG2 cells they inhibited the cell viability in concentration dependent manner (figure 8). These results suggested that these compounds are less effective against HepG2 cells compared to LNCaP cells (figure 8). For LNCaP cells, the estimated IC_{50} values of for present complexes were 44.12 µg/mL, 31.67 µg/mL and 71.38 µg/mL, respectively. The investigated compounds are more cytotoxic than HL and these results reveal that the cytotoxic activity increases when ligand are coordinated to the metal ion [77]. Probably, the high cytotoxicity of the compounds may be related to the intercalation of each metal complex with nitrogen bases of DNA tumor cells, causing greater conformational changes in the double-helix of DNA and then producing cell death [78]. On the other hand, these compounds were more cytotoxic compared with the toxic activity shown by *cis*-platin assayed in (HL60) human leukemia cells [17] and to Pt(II) and Pd(II) complexes with phenylacetaldehyde thiosemicarbazone ligands assayed in the K562 human chronic myelogenous leukemia cell line [79]. Cell viability results speculated that synthesized compounds may be further optimized and employed as promising anticancer agents.

4. Conclusion

We have synthesized and characterized three nickel(II) [$Ni(L)_2$] (**1**), and copper(II) [$Cu(L)_2$] (**2a**) and [$Cu(L)_2$] (**2b**) complexes which are formed through coordination of (E)-1-(2-methoxybenzylidine)-4-phenylethiosemicarbazone (HL) as bidentate N,S-ligand. Single-crystal analysis of synthesized complexes display a distorted tetrahedral and/or square planar *trans*-[MN_2S_2] coordination whose M(II) atoms lie on the center of symmetry. The Schiff base (HL) was prepared by the condensation of 4-phenyl thiosemicarbazide and 2-methoxybenzaldehyde in 1:1 molar ratio. Protein binding study of metal complexes indicated that a strong interaction has occurred between the metal complexes and BSA. Complex **1** shows a little higher free binding energy (-8.3 kcal/mol) with docked target DNA as compared to **2a**, which shows -8 kcal/mol binding free energy.

Supplementary materials

CCDC 1565755, 1836258 and 1837668 contain the supplementary crystallographic data for **1**, **2a** and **2b**, respectively. Copies of this information can be obtained free of charge via http://www.ccdc.cam.ac.uk/conts/retrieving.html/datarequest/cif, or from the Cambridge Crystallographic Data Centre, 12 Union Road, Cambridge CB2 1EZ, UK; Fax: (+44)-1223-336033 or E-mail: deposit@ccdc.cam.ac.uk.

Acknowledgements

Authors thank the Sophisticated Analytical Instrument Facility (SAIF), STIC Cochin for single crystal data collection of [$Ni(L)_2$] (**1**), and SAIF IIT Patna for [$Cu(L)_2$] (**2a**) and [$Cu(L)_2$] (**2b**). Financial assistance received from the Council of Scientific and Industrial Research (CSIR), New Delhi, India (Grant No. 01(2856)/16/EMR-II) is gratefully acknowledged. B. Mohan and Noorussabah acknowledge CSIR and TEQIP-II, NIT Patna, respectively, for their fellowships.

References

[1] A.N. Campbell, S.S. Stahi. *Acc. Chem. Res.*, **45**, 851 (2012).

[2] B. Su, Z.-C. Cao, Z.-J. Shi. *Acc. Chem. Res.*, **48**, 886 (2015).

[3] S. Stahi, J.A. Labinger, J.E. Bercaw. *Angew. Chem. Int. Ed.*, **37**, 2181 (1998).

[4] A. Rovasio, L. Boggioni. *Catal. Met. Complexes*, **35**, 27 (2011).

[5] S.S. Bhut, A.A. Kumbhar, H. Heptullah, A.A. Khan, V.V. Gobre, S.P. Gejji, V.G. Purani. *Inorg. Chem.*, **50**, 545 (2011).

[6] V. Rajeniran, R. Karthik, M. Palaniandavar, V.S. Periasamy, M.A. Akbarsha, B.S. Srinag, H. Krishnamurthy. *Inorg. Chem.*, **46**, 8208 (2007).

[7] J.S. Casas, M.S. Garcia-Tasende, J. Sordo. *Coord. Chem. Rev.*, **209**, 197 (2000).

[8] P.P. Netalkar, S.P. Netalkar, V.K. Revankar. *Transition Met. Chem.*, **39**, 519 (2014).

[9] D. Mishra, S. Naskar, M.G.B. Drew, S.K. Chattopadhyay. *Inorg. Chim. Acta*, **359**, 585 (2006).

[10] K.S. AbouMelha. *J. Enz. Inhib. Med. Chem.*, **23**, 493 (2008).

[11] Z. Afrasiabi, E. Sinn, S. Padhye. S. Dutta, S. Padhye, C. Newton, C.E. Anson, A.K. Powell. *J. Inorg. Biochem.*, **95**, 306 (2003).

[12] (a) R. Katwal, H. Kaur, B.K. Kapur. *Sci. Rev. Chem. Commun.*, **3**, 1 (2013). (b) D. Kovala-Demertzi, A. Boccarelli, M.A. Demertzis, M. Coluccia. *Chemotherapy*, **53**, 148 (2007). (c) J.P. Scovill, D.L. Klayman, C.F. Franchino. *J. Med. Chem.*, **25**, 1261 (1982). (d) A.G. Quiroga, J.M. Perez, I. Lopez-Solera, J.R. Masaguer, A. Luque, P. Roman, A. Edwards, C. Alonso, C.N. Ranninger. *J. Med. Chem.*, **41**, 1399 (1998). (e) R.F.F. Costa, A.P. Rebolledo, T. Matencio, H.D.R. Calado, J.D. Ardisson, M.E. Cortes, B.L. Rodrigues, H. Beraldo. *J. Coord. Chem.*, **58**, 1307 (2005).

[13] P. Anita, N. Chitrapriya, Y.J. Jang, P. Vishwanathamurthi. *J. Photochem. Photobiol. B*, **129**, 17 (2013).

[14] A. Basu, D. Thiyagarajan, C. Kar, A. Ramesh, G. Das. *RSC Adv.*, **3**, 14088 (2013).

[15] M.S. Bakkar, M. Yamin Siddiqi, M.S. Monshi. *Synth. React. Inorg. Met.-Org. Nano-Met. Chem.*, **33**, 1157 (2003).

[16] R.M. El-Shazly, G.A.A. Al-Hazmi, S.E. Ghazy, M.S. El-Shahawi, A.A. El-Asmy. *J. Coord. Chem.*, **59**, 845 (2006).

[17] H. Beraldo. *Quimica Nova*, **27**, 461 (2004).

[18] A.G. Quiroga, J.M. Perez, I. Lopez-Solera, E.I. Monterno, J.R. Masaguer, C. Alonso, C.N. Ranninger. *J. Inorg. Biochem.*, **69**, 275 (1998).

[19] K. Sampath, S. Sathiyaraj, C. Jayabalakrishnan. *Spectrochim. Acta, Part A*, **115**, 287 (2013).

[20] J.S. Casas, V. Castano, M.C. Cifuentes, A. Sanchez, J. Sordo. *Polyhedron*, **21**, 1646 (2000).

[21] (a) C. Paek, S.O. Kong, J. Ko, P.J. Carroll. *Organometallics*, **16**, 1503 (1997). (b) C. Paek, S.O. Kong, J. Ko, P.J. Carroll. *Organometallics*, **16**, 2110 (1997). (c) C. Paek, S.O. Kong, J. Ko, P.J. Carroll. *Organometallics*, **16**, 4755 (1997). (d) C. Paek, S.O. Kong, J. Ko, P.J. Carroll. *Organometallics*, **16**, 5522 (1997).

[22] A. Castineiras, E. Bermejo, D.X. West, A.K. El-Sawaf, J.K. Swearingen. *Polyhedron*, **17**, 2751 (1998).

[23] J.S. Casas, E.E. Castellano, A. Macıas, Rodrıguez-Arguelles, A. Sanchez, J. Sordo. *J. Chem. Soc., Dalton Trans.*, 1293 (1993).

[24] D. Mishra, S. Naskar, M.G.B. Drew, S.K. Chattopadhyay. *Polyhedron*, **24**, 1861 (2005).

[25] Y. Liu, H. Chao, Y. Yuan, H. Yu, L. Ji. *Inorg. Chim. Acta*, **359**, 3807 (2006).

[26] H. Khan, A. Badshah, Z.-U. Zia-Ur-Rehman, U.A. Rana, S.U.D. Khan, Z. Iqbal, N. Ahmad. *Polyhedron*, **39**, 1 (2012).

[27] H. Khan, A. Badshah, G. Murtaz, M. Said, J.U. Rehman, C. Neuhausen, M. Todoroya, B.J. Jean-Claude, I.S. Butler. *Eur. J. Med. Chem.*, **46**, 4071 (2011).

[28] S.M. Meier, M. Hanif, W. Kandioller, B.K. Keppler, C.G. Hartinger. *J. Inorg. Biochem.*, **108**, 91 (2012).

[29] D. Debouis, I.P. Troitsky, M.J. Bellousoff, L. Spiccis, B. Graham. *Coord. Chem. Rev.*, **256**, 897 (2012).

[30] L. Marcelis, J. Ghesquiere, K. Garnir, A.K.D. Mesmaeker, C. Moucheron. *Coord. Chem. Rev.*, **256**, 1569 (2012).

[31] C. Marzano, M. Pellei, F. Tisano, C. Santini. *Anticancer Agents. Med. Chem.*, **9**, 185 (2009).

[32] M. Das, R. Nasani, M. Saha, S.M. Mobin, S. Mukhopadhyay. *Dalton Trans.*, **44**, 2299 (2015).

[33] C. Balakrishnan, S. Natarajan, M.A. Neelakantan. *RSC Adv.*, **6**, 102482 (2016).

[34] T. Peters, *All About Albumin: Biochemistry Genetics and Medical Applications*, Academic Press, San Diego, CA (1995).

[35] (a) M. Asadi, Z. Asadi, L. Zarei, S.B. Sadi, Z. Amirghofran. *Spectrochim. Acta, Part A*, **133**, 697 (2014). (b) P. Li, M.J. Liu, M. Hong, S. Cheng, J.M. Dou. *J. Inorg. Biochem.*, **137**, 101 (2014). (c) M.J. Niu, Z. Li, H.H. Li, X. Li, J.M. Dou, S.N. Wang. *RSC Adv.*, **5**, 37085 (2015). (d) M.J. Niu, M. Hong, G.L. Chang, X. Li, Z. Li. *J. Photochem. Photobiol. B*, **148**, 232 (2015).

[36] M. Muralisankar, J. Haribabu, N.S.P. Bhuvanesh, R. Karvembu, A. Sreekanth. *Inorg. Chim. Acta*, **49**, 82 (2016).

[37] M. Muralisankar, S.M. Basheer, J. Haribabu, N.S.P. Bhuvanesh, A. Sreekanth. *Inorg. Chim. Acta*, **466**, 61 (2017).

[38] S. Bharti, M. Choudhary, B. Mohan, S.P. Rawat, S.R. Sharma, K. Ahmad. *J. Mol. Struct.*, **1146**, 137 (2018).

[39] S. Bharti, M. Choudhary, B. Mohan. *J. Coord. Chem*, **71**, 284 (2018).

[40] B. Mohan, A. Jana, N. Das, S. Bharti, M. Choudhari. *J. Mol. Struct.*, **1171**, 94 (2018).

[41] B. Mohan, A. Jana, N. Das, S. Bharti, M. Choudhari, S. Muhammad, S. Kumar, A.G. Al-Sehemi, H. Algarn. *Inorg. Chim. Acta*, **484**, 148 (2019).

[42] D. Bradley, G. Williams, M. Lawton. *J. Org. Chem.*, **75**, 8351 (2010).

[43] A.B. Pangborn, M.A. Giurdello, R.H. Grubbs, R.K. Rosen, F.J. Timers. *Organometallics*, **15**, 1518 (1996).

[44] M. Muralisankar, S. Sujith, N.S.P. Bhuvanesh, R. karvembu, A. Sreekanth. *Polyhedron*, **118**, 103 (2016).

[45] J. Haribabu, G.R. Subhashree, S. Saranva, K. Gumathi, R. Karvembu, D. Gayatri. *J. Mol. Struct.*, **1110**, 185 (2016).

[46] G.M. Sheldrick. *Acta Cryst., Sect. A*, **64**, 112 (2008).

[47] G.M. Sheldrick. *Acta Cryst., Sect. C*, **71**, 3 (2015).

[48] G.W. Zhang, Q.M. Que, J.H. Pan, J.B. Guo. *J. Mol. Struct.*, **881**, 132 (2008).

[49] G.M. Morris, R. Huey, N. Lindstrom, M.F. Sanner, R.K. Belew, D.S. Goodsell, A.J. Olson. *J. Comp. Chem.*, **30**, 2785 (2009).

[50] O. Trott, A.J. Olson. *J. Comp. Chem.*, **31**, 455 (2010).

[51] W. DeLano, *The PyMOL Molecular Graphics System, Version 1.2 r3pre, Schrödinger, LLC.* There is no corresponding record for this reference (2002).

[52] D.S. Biovia, *Discovery Studio Modeling Environment*, San Diego: Dassault Systemes (2015).

[53] R.A. Laskowski, M.B. Swindells. *J. Chem. Info. Model.*, **51**, 2778 (2011).

[54] P. Khan, S. Rahman, A. Queen, S. Manzoor, F. Naz, G.M. Hasan, S. Luqman, J. Kim, A. Islam, F. Ahmad, M.I. Hassan. *Sci. Rep.*, **7**, 9470 (2017).

[55] A. Queen, P. Khan, D. Idrees, A. Azam, M.I. Hassan. *Int. J. Biol. Macromol.*, **106**, 840 (2018).

[56] W.J. Geary. *Coord. Chem. Rev.*, **7**, 81 (1971).

[57] (a) S. Blanchard, F. Neese, E. Bothe, E. Bill, T. Weyhermuller, K. Wieghardt. *Inorg. Chem.*, **44**, 3636 (2005). (b) A.A. Nejo, G.A. Kolawole, M.C. Dumbele, A.R. Opoku. *J. Coord. Chem.*, **63**, 4367 (2010).

[58] R.N. Patel, Y.P. Singh, Y. Singh, R.J. Butcher, J.P. Jasinski. *Polyhedron*, **129**, 164 (2017).

[59] M. Salehi, F Rahimifar, M. Kubicki, A. Asadi. *Inorg. Chim. Acta*, **443**, 28 (2016).

[60] S. Saha, S. Jana, S. Gupta, A. Ghosh, H.P. Nayek. *Polyhedron*, **107**, 183 (2016).

[61] V. Kuchtanin, L. Klescikova, M. Soral, R. Fischer, Z. Ruzickova, E. Rakovsky, J. Moncol, P. Segla. *Polyhedron*, **117**, 90 (2016).

[62] S. Kundu, A.K. Pramanik, A.S. Mondal, T.K. Mondal. *J. Mol. Struct.*, **1116**, 1 (2016).

[63] T. Akitsu, Y. Einaga. *Polyhedron*, **24**, 1869 (2005).

[64] S. Sangeeta, K. Ahmad, N. Noorussabah, S. Bharti, M.K. Mishra, S.R. Sharma, M. Choudhary. *J. Mol. Struct.*, **1556**, 1 (2018).

[65] S. Sangeeta, K. Ahmad, N. Noorussabah, S. Bharti, M.K. Mishra, S.R. Sharma, M. Choudhary. *J. Mol. Struct.*, **1149**, 183 (2017).

[66] P.P. Netalkar, S.P. Netalkar, V.K. Revankar. *Polyhedron*, **100**, 215 (2015).

[67] I.T. Ahmad. *J. Coord. Chem.*, **61**, 1730 (2008).

[68] T.S. Lobana, R. Sharma, G. Bawa, S. Khanna. *Coord. Chem. Rev.*, **253**, 977 (2009).

[69] V. Mahalingam, N. Chitrapriya, F.R. Fronczek, K. Natarajan. *Polyhedron*, **29**, 3363 (2010).

[70] S. Chandra, A.K. Sharma/ *Spectrochim. Acta*, **74A**, 271 (2009).

[71] (a) H. Beraldo, R. Lima, L.R. Teixeira, A.A. Moura, D.X. West. *J. Mol. Struct.*, **557**, 99 (2001). (b) W.F. Beraldo, L.R. Nacif, L.R. Texeira, J.S. Reboucas. *Transition Met. Chem.*, **27**, 85 (2002).

[72] X.L. Wang, H. Chao, H. Li, X.L. Hong, Y.J. Liu, L.F. Tan, L.N. Ji. *J. Inorg. Biochem.*, **98**, 1143 (2004).

[73] P. Krishnamoorthy, P. Sathyadevi, A.H. Cowley, R. Butorac, N. Dharmaraj. *Eur. J. Med. Chem.*, **46**, 3376 (2011).

[74] D.S. Raja, N.S.P. Bhuvanesh, K. Natarajan. *Dalton Trans.*, **42**, 4365 (2012).

[75] M. Ahmad, H. Pervez, Z.S. Ziab, M. Yaqub, M.M. Naseer, S.U. Khan, J. Iqbal. *RSC Adv.*, **6**, 60826 (2016).

[76] T. Mosmann. *J. Immunol. Methods*, **65**, 55 (1983).

[77] N. Bahrti, F. Naqvi, A. Azam. *Bioinorg. Med. Chem. Lett.*, **13**, 689 (2003).

[78] J.A. Hickman. *Cancer Metastasis Rev.*, **11**, 121 (1992).

[79] N. Gokhale, S. Padhye, D. Rathbone. *Inorg. Chem. Commun.*, **4**, 26 (2001).

Table 1. Crystal data and structure refinement of **1**, **2a** and **2b**.

	1	**2a**	**2b**
Empirical formula	$C_{30}H_{28}NiN_6O_2S_2$	$C_{30}H_{28}CuN_6O_2S_2$	$C_{30}H_{28}CuN_6O_2S_2$
Formula weight	627.41	632.25	632.25
Temperature (K)	296(2)	150	293
Wavelength (Å)	0.71073	0.71073	0.71073
Crystal system	Orthorhombic	Orthorhombic	Monoclinic
Space group	Pbca	Pbca	P2*1*/*c*
Unit cell dimensions			
a (Å)	15.4786(11)	15.507(3)	19.141(7)
b (Å)	7.6422(5)	7.5988(16)	7.667(3)
c (Å)	24.613(2)	24.876(5)	22.470(9)
α (°)	90	90	90
β (°)	90	90	104.803(11)
γ (°)	90	90	90
Volume ($Å^3$)	2911.4(4)	2931.3(11)	3188(2)
$D_{calc.}$ (Mg/m^3)	1.431	1.433	1.317
Z	4	4	4
Absorption coefficient (mm^{-1})	0.849	0.926	0.857
F (000)	1304	1308	1308
Crystal size (mm)	0.30 x 0.20 x 0.20	0.20 x 0.20 x 0.15	0.20 x 0.25 x 0.10
ϑ Range for data collection (°)	1.65 to 28.38	2.627 to 28.394	2.500 to 28.388
Limiting index	-20<=h<=16 -10<=k<=10 -32<=l<=31	-19<=h<=20 -10<=k<=10 -33<=l<=33	-25<=h<=25 -10<=k<=10 -29<=l<=29
Reflections collected/unique [R_{int}]	21911/3632[0.0416]	54434/3663[0.0794]	69403/7921[0.1405]
Completeness to θ	28.38 - 99.6%	28.394 - 99.8%	28.388 - 99.0%
Absorption correction	Semi-empirical from equivalents	Semi-empirical from equivalents	Semi-empirical from equivalents
Max. and min. transmission	0.8486 and 0.7848	0.929 and 0.887	0.746 and 0.680
Refinement method	Full-matrix least-squares	Full-matrix least-squares	Full-matrix least-squares
Data / restraints / parameters	3632 / 0 / 189	3663 / 0 / 201	7921 / 0 / 372
Goodness-of-fit on F^2	1.138	1.043	1.071
Final R indices [I>2 σ(I)]	R_1 = 0.0407 $_wR_2$ = 0.1035	R_1 = 0.0403 $_wR_2$ = 0932	R_1 = 0.0934 $_wR_2$ = 0.1857

Table 2. Selected bond lengths (Å) and angles (°) for **1**, **2a** and **2b**.

	1		**2a**		**2b**	
Bond length	Ni(1)-N(3)	1.9127(17)	S(1)-Cu(1)	2.2556	S(1)-Cu(1)	2.225(2)
	Ni(1)-S(1)#1	2.1708(6)	N(3)-Cu(1)	2.008	N(3)-Cu(1)	1.987(3)
	Ni(1)-S(1)	2.1708(6)	S(1)-C(1)	1.741(2)	S(2)-Cu(1)	2.235(2)
	Ni(1)-N(3)#1	1.9128(17)	O(1)-C(9)	1.364(3)	N(6)-Cu(1)	1.993(4)
Bond angles	N(3)-Ni(1)-N(3)#1	180.00(10)	S(1)-Cu(1)-N(3)	83.91	S(1)-Cu(1)-N(3)	85.2 (1)
	N(3)-Ni(1)-S(1)#1	85.28(6)	S(1)-Cu(1)-S(1)	180.00	S(1)-Cu(1)-S(2)	156.32(6)
	N(3)#1-Ni(1)-S(1)#1	94.72(6)	S(1)-Cu(1)-N(3)	96.09	S(1)-Cu(1)-N(6)	100.1(1)
	N(3)-Ni(1)-S(1)	94.72(6)	N(3)-Cu(1)-S(1)	96.09	N(3)-Cu(1)-S(2)	97.8(1)
	N(3)#1-Ni(1)-S(1)	85.28(6)	N(3)-Cu(1)-N(3)	180.00	N(3)-Cu(1)-N(6)	159.6(2)
	S(1)#1-Ni(1)-S(1)	180.0	S(1)-Cu(1)-N(3)	83.91	S(2)-Cu(1)-N(6)	85.2(1)

Symmetry transformations used to generate equivalent atoms: #1 -x,-y+2,-z+1 for **1**.

Table 3. Protein binding constant (K_b), quenching constant (K_{SV}) and number of binding sites (n) of **1** and **2a**.

Complex	K_b (M^{-1})	K_{SV} (M^{-1})	n
1	2.38×10^5	0.015×10^5	1.245
2a	7.73×10^2	0.005×10^5	0.709

Table 4. Binding affinity of **1** and **2a** with the DNA generated from molecular docking, and interacting residues of DNA (*Note: C9(A) means, the cytosine at 9th position of strand A*).

Complex	Affinity (kcal/mol)	Interacting residues
1	-8.3	C3(A), G4(A), A5(A), A6(A), T7(A), G16(B), A17(B), A18(B), T19(B) and T20(B)
2a	-8.0	C9(A), G10(A), C11(A), G12(A), G14(B), C15(B), G16(B), A17(B) and A18(B)

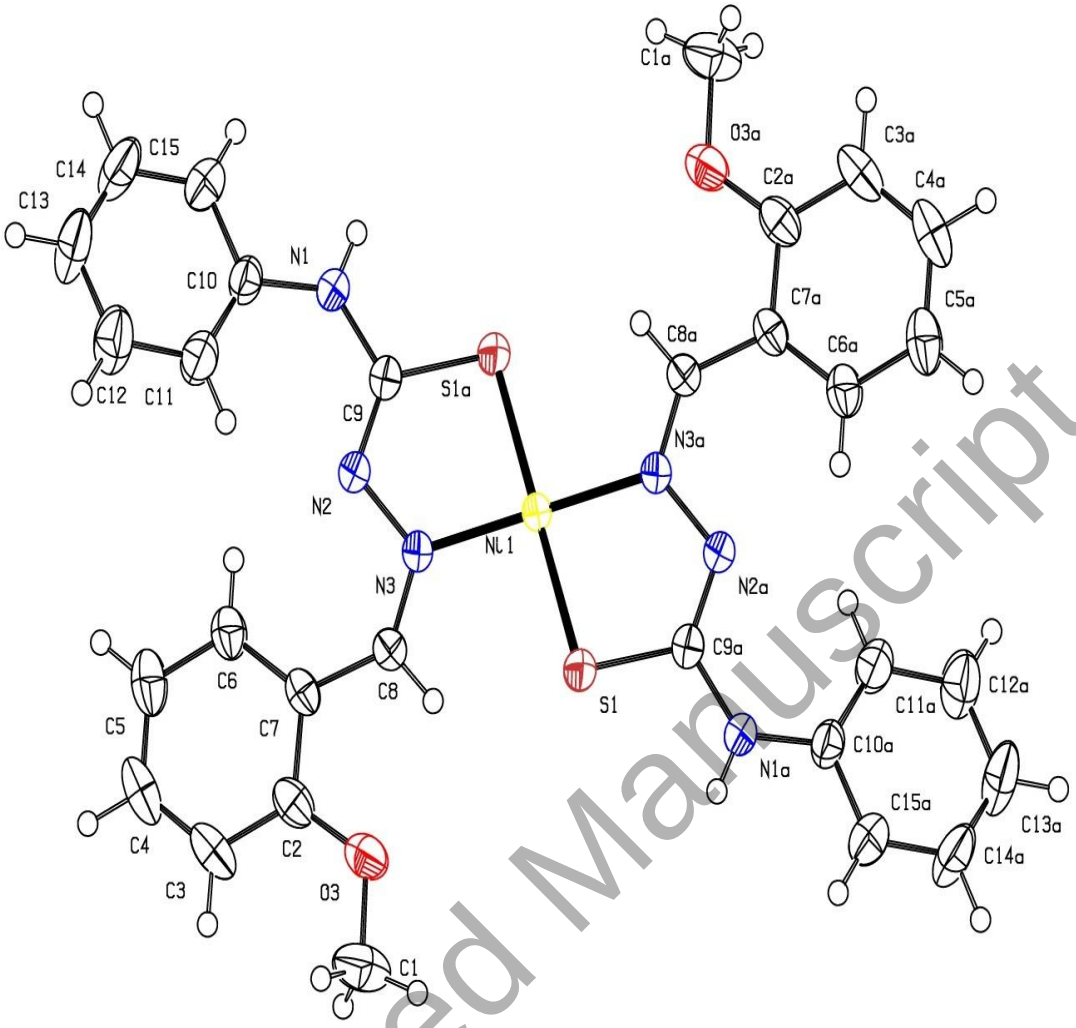

Figure 1. ORTEP structure of **1** with 50% thermal ellipsoid and with atom numbering scheme.

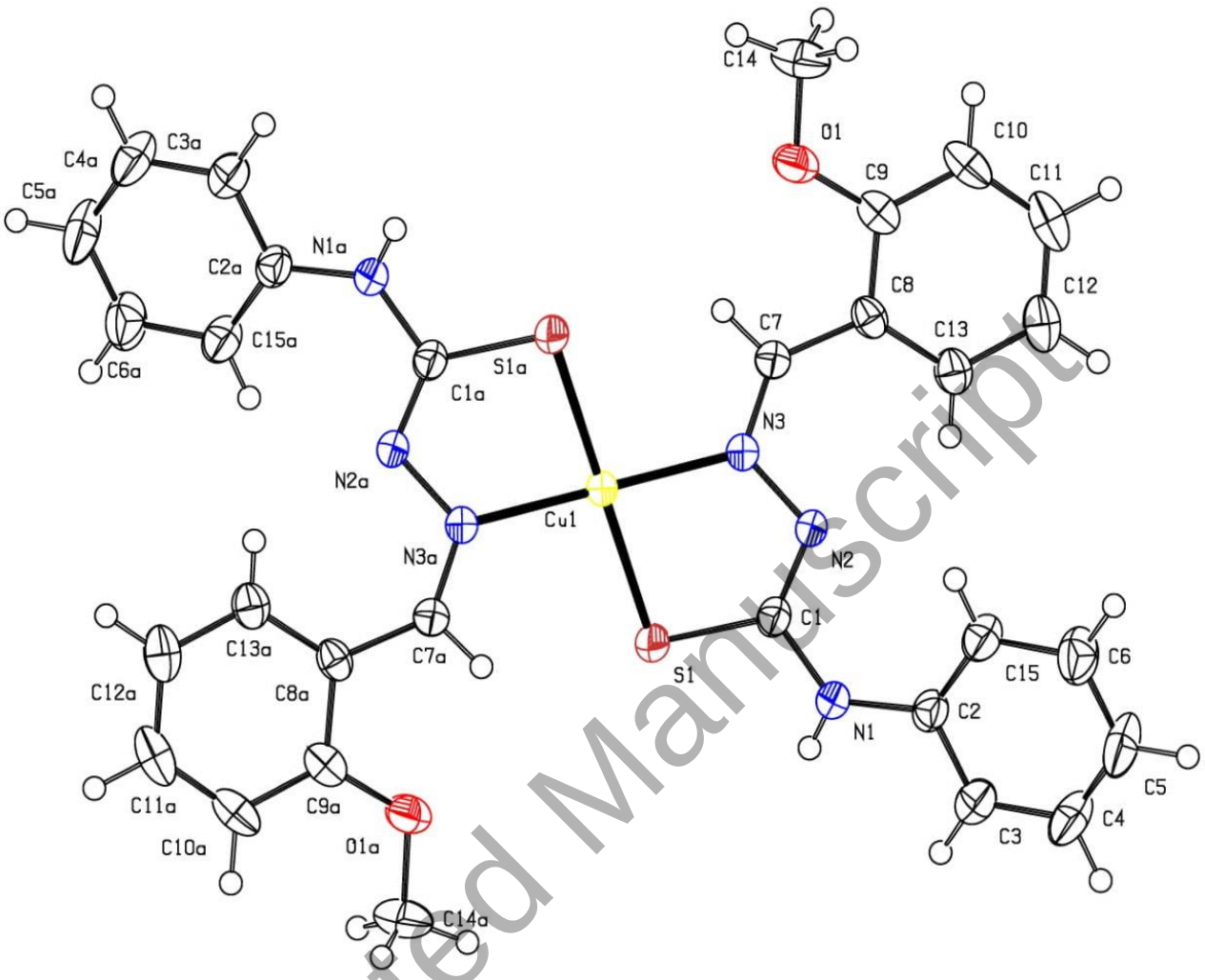

Figure 2. ORTEP structure of **2a** with 30% thermal ellipsoid and with atom numbering scheme.

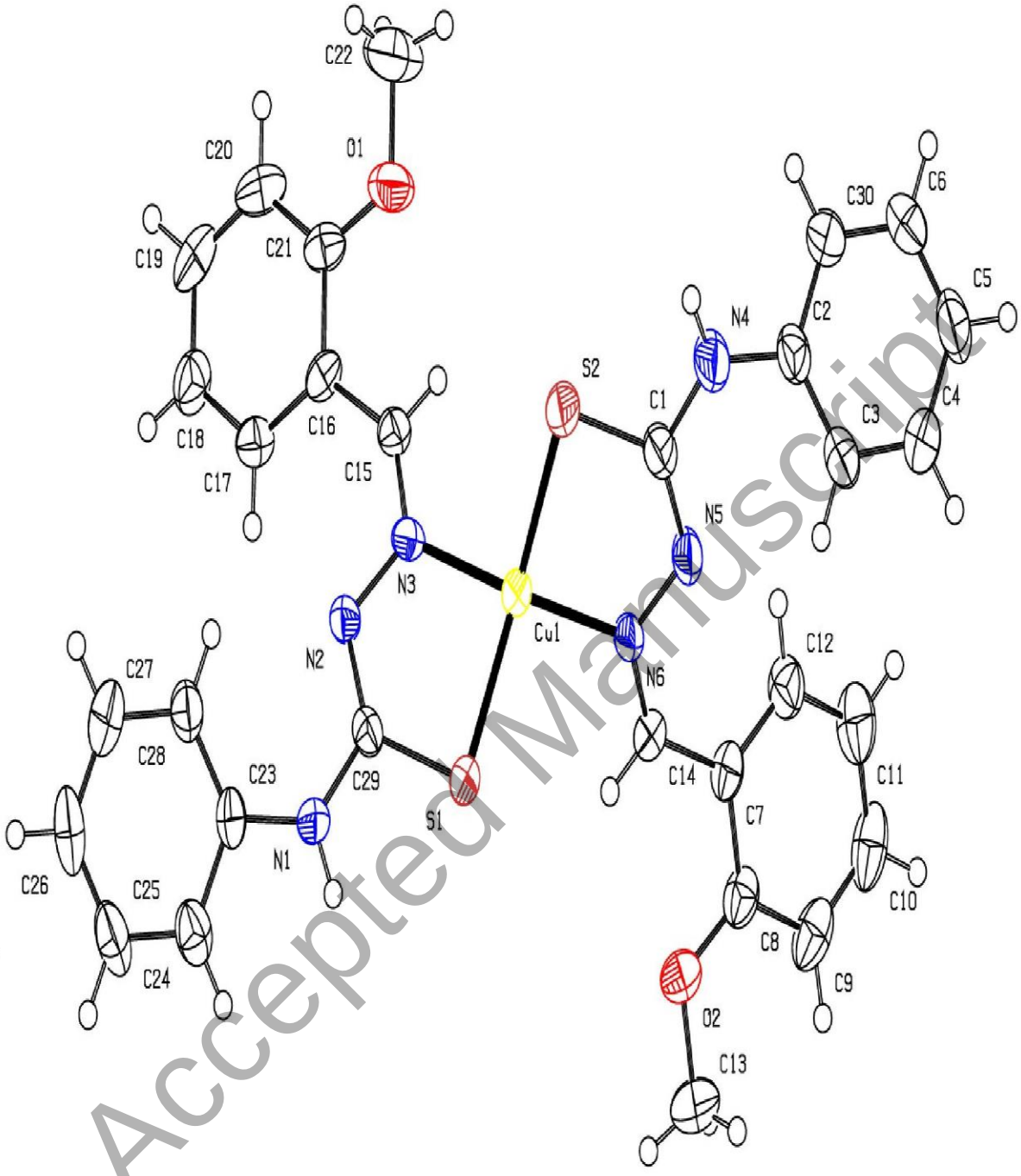

Figure 3. ORTEP structure of **2b** with 50% thermal ellipsoid and with atom numbering scheme.

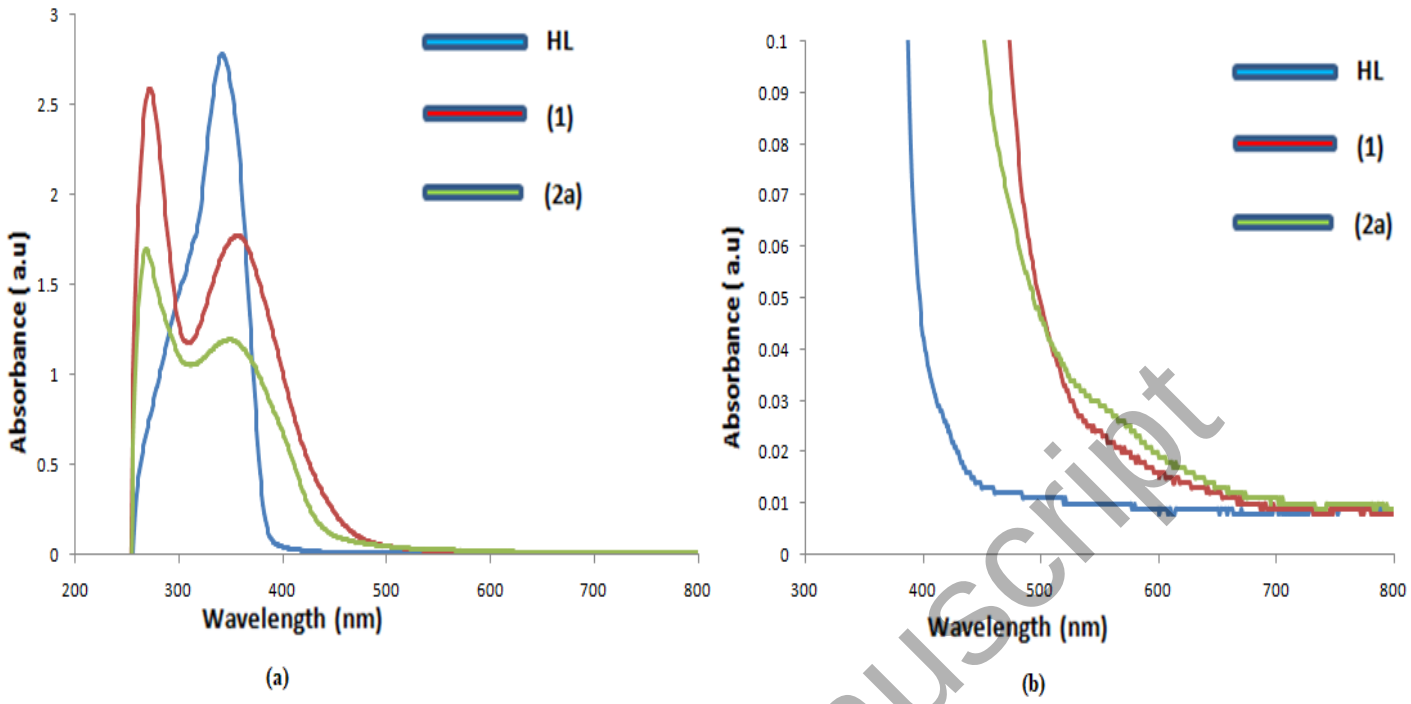

Figure 4. (a) The UV-visible absorption spectra of HL and its complexes **1** and **2a**; (b) UV-visible absorption spectra of HL and its complexes with expanded the *y*-axis from 300-800 nm.

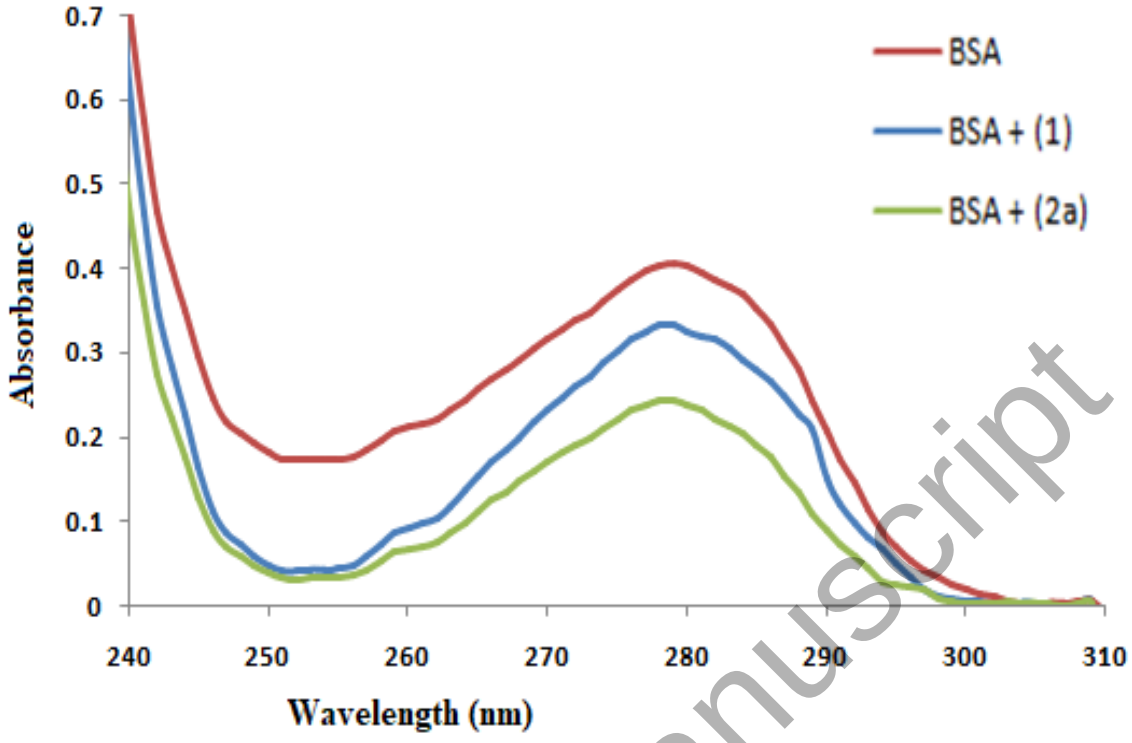

Figure 5. UV absorption spectra of BSA (10 μM) and BSA with **1** and **2a**.

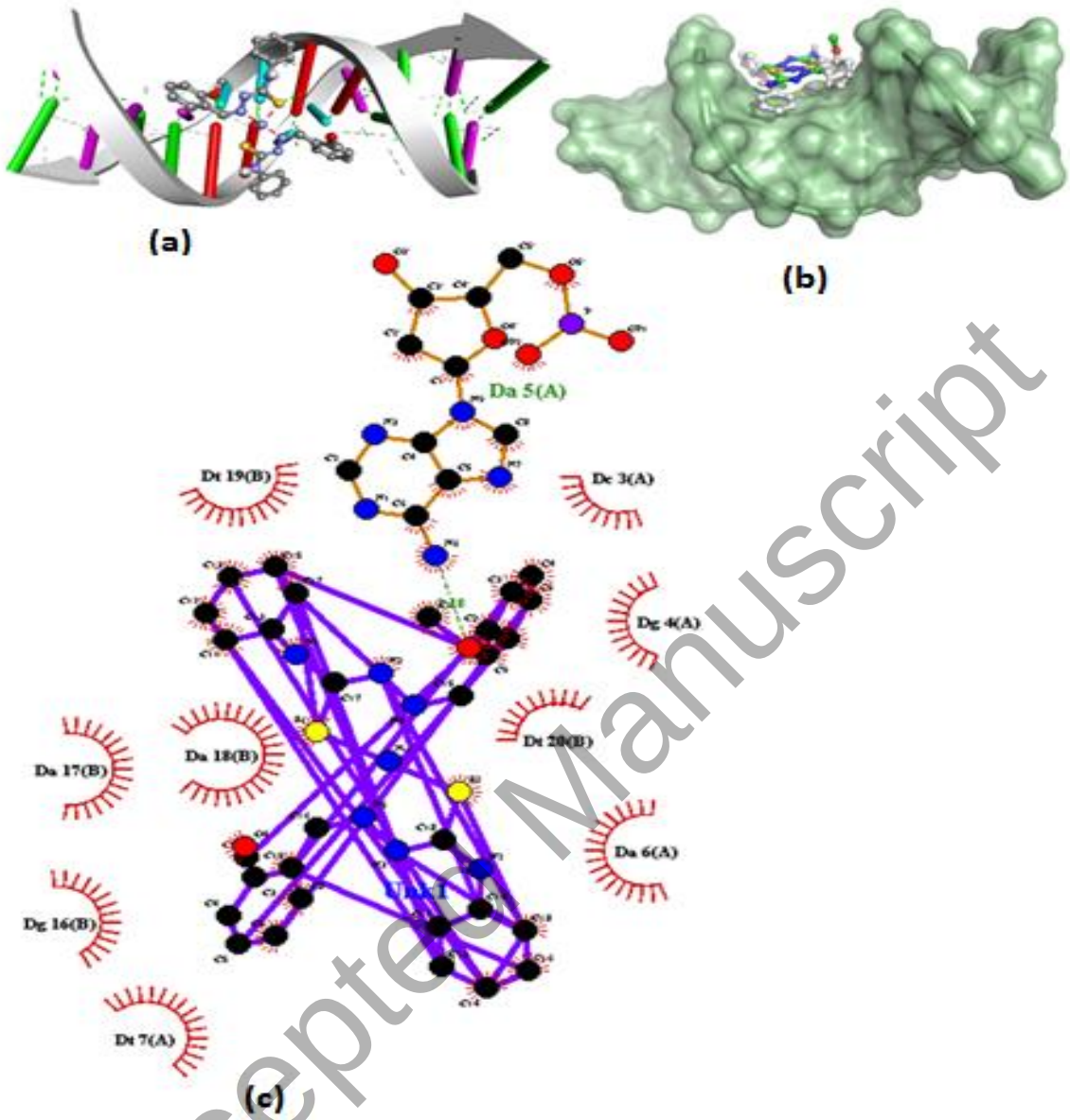

Figure 6. The interaction between DNA and **1**; (a) docked conformation of **1** with DNA; (b) **1** docked into the DNA groove; (c) interacting residues of DNA with **1**.

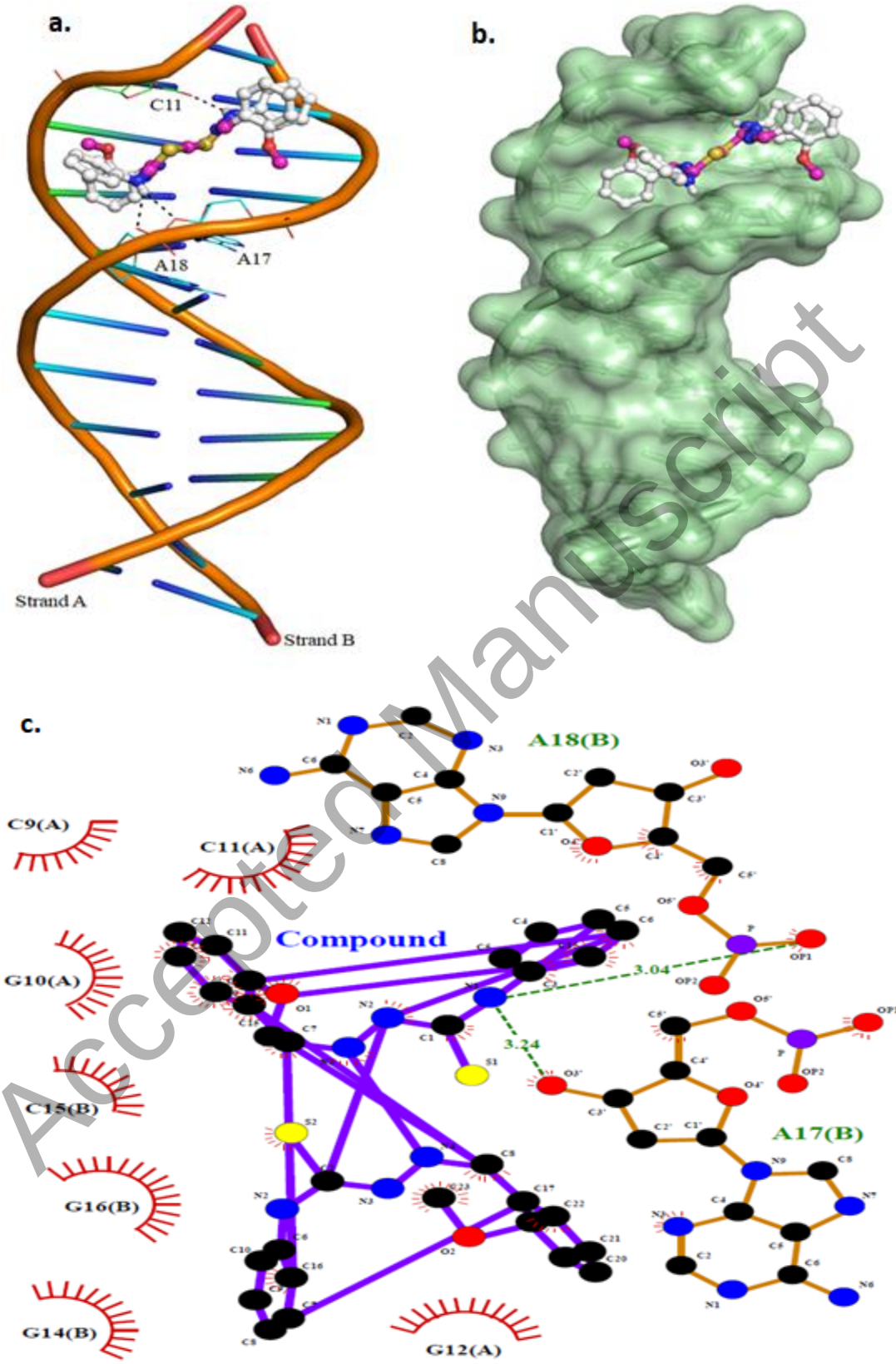

Figure 7. The interaction between DNA and **2a**; (a) docked conformation of **2a** with DNA; (b) **2a** docked into the DNA groove; (c) interacting residues of DNA with **2a**.

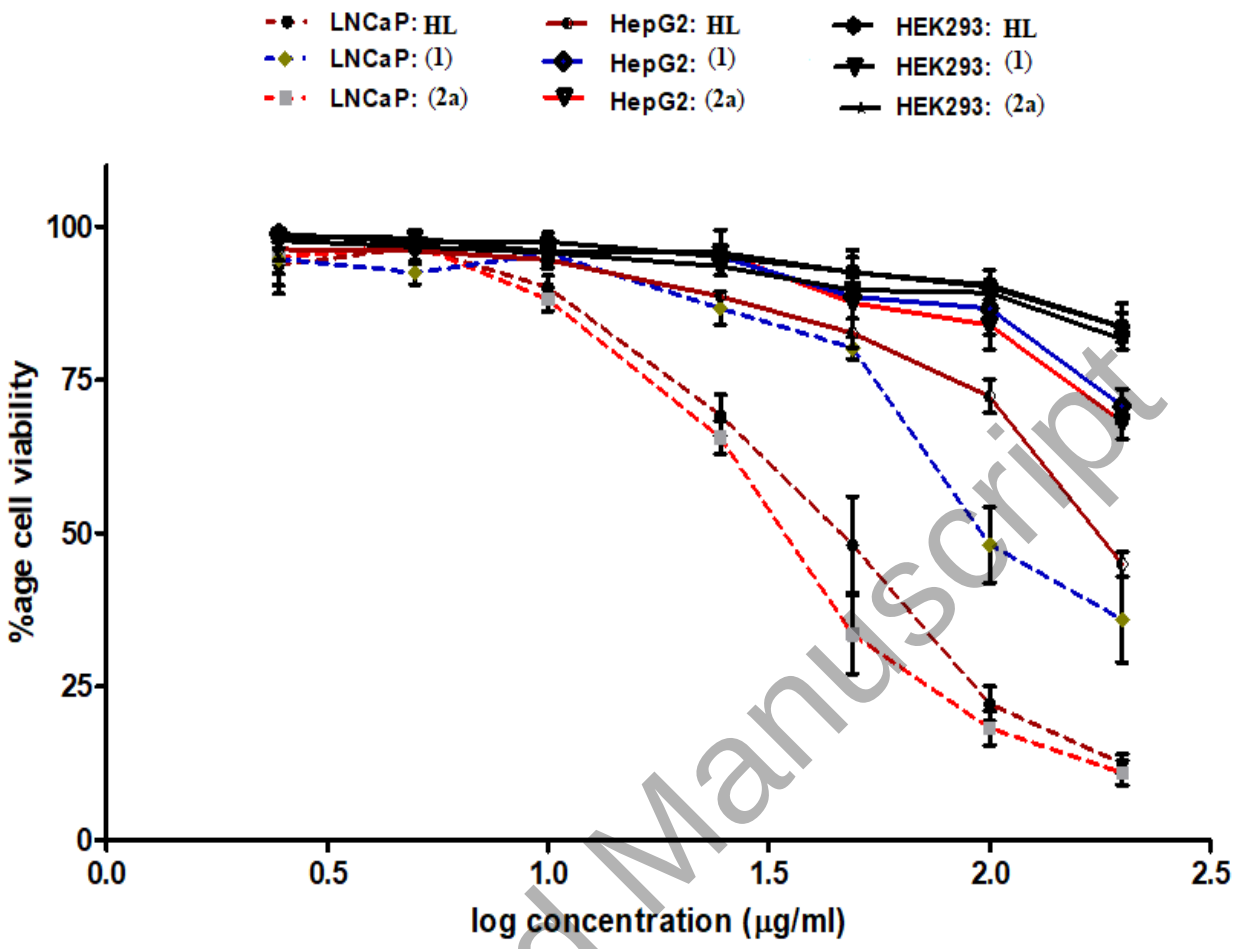

Figure 8. Cell viability of HEK-293, LNCaP and HepG2 cells in the presence of increasing concentrations of synthesized compounds as measured by MTT assay. The percentage cell viability was calculated with respect to the control cells (cells treated with media only) and plotted as a function of concentration.